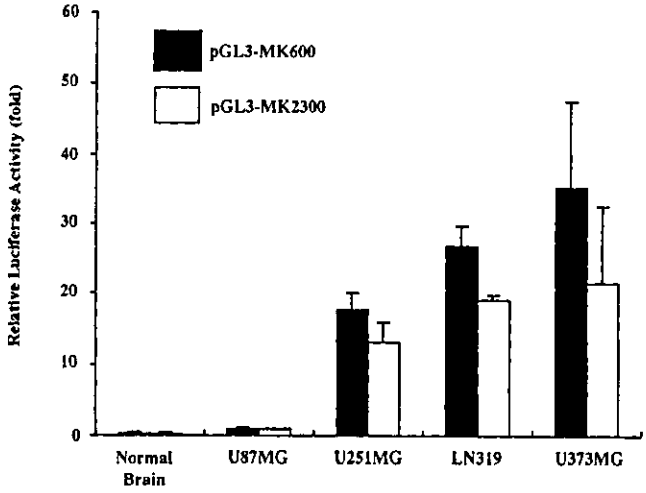

Figure 3. Transcriptional activity of the *MK* promoter. Luciferase activity of reporter plasmids with the *MK* promoter was assayed in MK-positive glioma cells (U251MG, LN319 and U373MG), and MK-negative cells (primary normal brain cells and U87MG). The 600-bp and 2300-bp fragments of the *MK* promoter were inserted into luciferase reporter plasmid (pGL3-MK600, pGL3-MK2300). Bars, means ± SD.

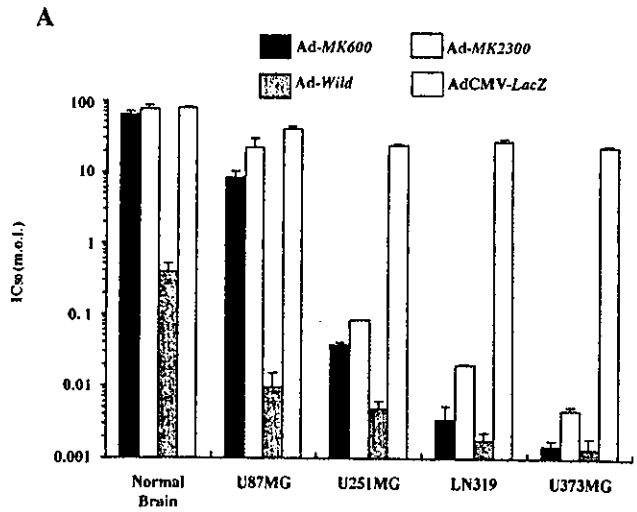

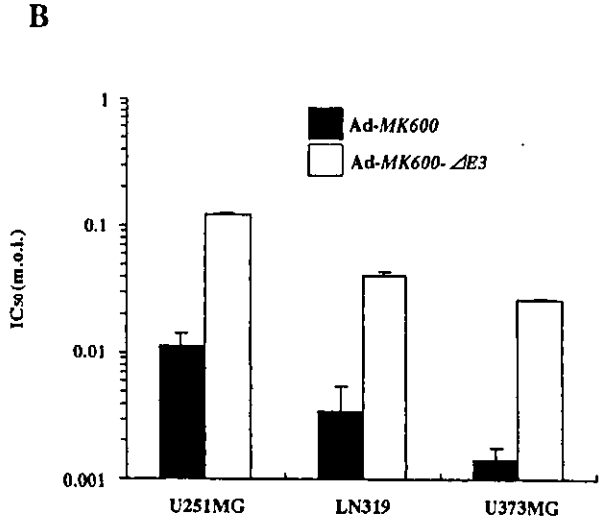

Figure 5. Cytotoxic effect induced by the infection with Ad-*MK* in glioma cells. (A), Cells were infected with AdCMV-*LacZ*, Ad-*MK600*, Ad-*MK2300* or Ad-*Wild* for ten days. The IC_{50} (m.o.i.) was calculated. Bars, means ± SD. (B), Cytotoxic effect of adenoviral *E3* region on Ad-*MK600*. Three MK-positive cell lines were infected with Ad-*MK600* or Ad-*MK600-ΔE3*. The IC_{50} of each adenovirus was determined. Bars, means ± SD.

expression in human glioma cell lines and primary normal brain cells, cells were infected with Ad-*MK600* at 10 m.o.i. for 36 h. Expression of E1A protein was assessed by Western blot analysis as shown in Fig. 4. Ad-*MK600* produced obvious expression of E1A in the MK-positive cells, but not in the MK-negative cells. Although there was no detectable E1A expression in cells infected with AdCMV-*LacZ*, E1A was clearly expressed in all cells infected with Ad-*Wild*.

Selective cytotoxicity of Ad-MK on glioma cells in vitro. To evaluate the cytotoxicity of the *MK* promoter-dependent adenovirus *in vitro*, we evaluated IC_{50} (m.o.i.) of Ad-*MK600* and Ad-*MK2300* on glioma cell lines and primary normal brain cells. As shown in Fig. 5A, the IC_{50} of Ad-*MK600* was 0.037, 0.0035 and 0.0014 m.o.i. for U251MG, LN319 and

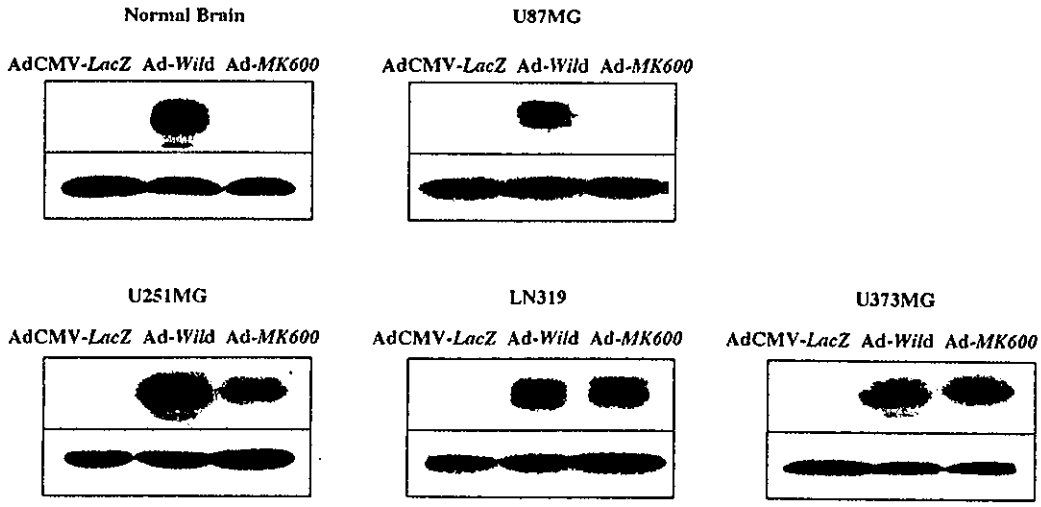

Figure 4. Expression of E1A in glioma cells. Cells were infected with AdCMV-*LacZ*, Ad-*Wild*, or Ad-*MK600*. Cell lysates from infected cells were subjected to Western blot analysis with anti-E1A antibodies. Top panel shows the band position of E1A protein and the ß-actin control is shown in bottom panel.

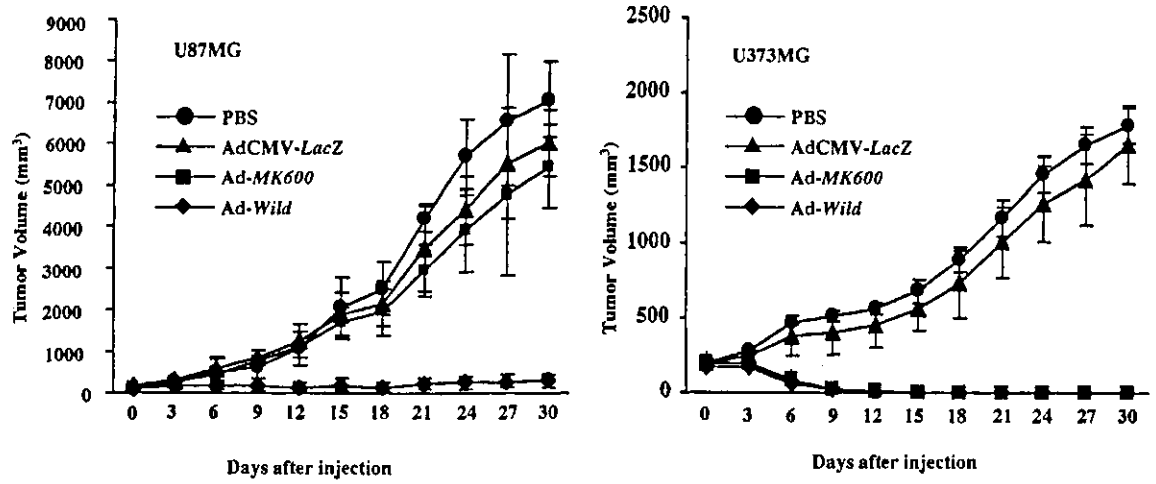

Figure 6. Effect on tumor growth from treatment with no virus (PBS), AdCMV-*LacZ*, Ad-*MK600* or Ad-*Wild*. U87MG or U373MG glioma cells ($1x10^7$) were injected s.c. into flanks of nude mice, followed by the intra-tumoral injection of adenoviruses. MK-positive U373MG tumor xenografts were effectively treated by a single dose of Ad-*MK600* (right), whereas MK-negative U87MG tumor xenografts were unaffected (left). Bars, means ± SD.

U373MG cells, respectively, with a mean value of 0.014 m.o.i., which was respectively 4500 times and 600 times lower than those for primary normal brain cells ($P<0.01$, unpaired t-test) and U87MG ($P<0.01$, unpaired t-test). In MK-positive cells, the IC_{50} of Ad-*MK600* was 4 times lower than that of Ad-*MK2300* ($P<0.01$, paired t-test). In contrast, the IC_{50} of AdCMV-*LacZ* did not differ significantly between cell lines. In MK-positive cells, the IC_{50} of Ad-*MK600* was 2100 times lower than that of AdCMV-*LacZ* ($P<0.01$, paired t-test). In MK-negative primary normal brain cells, the IC_{50} of both Ad-*MK* viruses were not significantly different from those of AdCMV-*LacZ*.

To explore the oncolytic role of the *E3* region in the context of Ad-*MK600*, we analyzed the difference of cytotoxic capacity between *E3*-intact Ad-*MK600* and *E3*-deleted Ad-*MK600-ΔE3* in MK-positive cells. Cytotoxic potency of Ad-*MK600* was 14 times that of Ad-*MK600-ΔE3* ($P<0.05$, unpaired t-test; Fig. 5B).

Treatment of glioma xenografts with Ad-MK600. To evaluate the therapeutic efficacy of Ad-*MK600 in vivo*, no vector (PBS), AdCMV-*LacZ*, Ad-*MK600* or Ad-*Wild* was injected into U87MG and U373MG glioma xenografts on day 0. As shown in Fig. 6, Ad-*MK600* and Ad-*Wild* completely eradicated the U373MG tumors ($P<0.001$, χ^2 test). In contrast, Ad-*MK600* did not significantly reduce the sizes of U87MG tumors compared with AdCMV-*LacZ*. However, Ad-*Wild* significantly reduced the size of U87MG tumors by 98% compared with AdCMV-*LacZ* ($P<0.001$, unpaired t-test).

Discussion

Tumor-selective oncolysis is key to the use of replicating viruses as cancer therapeutics. An appropriate promoter for malignant glioma has not yet been identified. Only nestin promoter and myelin basic protein promoter have reportedly been used to construct viral vectors for treatment of malignant glioma, but these vectors lack adequate tumor specificity and therapeutic effect for malignant glioma (2). Recently, the regulatory sequences of the human *MK* and *cox-2* genes have been used for transcriptional targeting of gene expression in the context of gene therapy, because overexpression of these genes has reportedly been observed in various types of malignant tumors, such as gastrointestinal, ovarian and breast cancer (6,10). In malignant glioma, it has been reported that MK and cox-2 expression correlate with malignancy in immunohistochemical, Western blot and Northern analysis (7,10). These reports involved qualitative analysis; there have been no reported quantitative analyses of expression of MK and cox-2 in malignant glioma. We report here, for the first time, the quantitative analysis of *MK* and *cox-2* expression in malignant glioma. In the present study, *MK* was overexpressed in malignant glioma tissues but *cox-2* was not. These findings indicate that transcriptional upregulation of the *MK* gene might be highly specific for malignant gliomas, compared with the *cox-2* gene. Furthermore, it has been reported that MK has good potential as a tumor marker in esophageal cancer, gastrointestinal cancer, pancreatic cancer and lung cancer (6). Although serum and cerebral spinal fluid levels of MK have not yet been identified in the patient with malignant glioma, our results indicate that MK might be feasible for a marker of malignant transformation in human glioma. Further analysis is required to determine the reliability, sensitivity and precision of MK as a marker of malignant transformation.

It has been reported that Ad-*MK* without the *E3* region in which E1A expression is driven by 2300 bp of the 5'-flanking region of the human *MK* gene, has been used for the treatment of neuroblastoma (11). However, the present results indicated that a 600-bp fragment of the *MK* promoter region activates transcription of the luciferase gene to a greater degree than a 2300-bp fragment. Furthermore, the oncolytic effect of Ad-*MK600* was 4 times that of Ad-*MK2300*. Yoshida *et al* (12) have reported that a 559-bp fragment of the *MK* gene activates transcription of the reporter gene more efficiently than a 2300-bp fragment in pancreatic cancer. These findings regarding *MK* promoter activity are consistent with the present results. In the present study, Ad-*MK600* had a

significant oncolytic effect that was 14 times that of Ad-*MK600-ΔE3*, indicating that *E3* is responsible for augmentation of the antitumor potency of CRAd.

The present is the first study of CRAd in which the cell-type specificity of the *MK* promoter was used to target malignant glioma. We found that Ad-*MK* selectively killed MK-positive glioma cells, but did not kill MK-negative primary normal brain cells. Additionally, in animal models, Ad-*MK600* completely eradicated MK positive-glioma xenografts. AdCMV-*LacZ* had minimum effect suggesting that the therapeutic effect of Ad-*MK600* was associated with viral replication, cell lysis and viral spread. In previous studies, replication-selective adenovirus without the *E1B 55-kDa* sequence (ONYX-015) (13) and replicative adenoviral vector expressing herpes simplex virus-thymidine kinase (14), which were used for treatment of malignant glioma, did not completely eradicate tumors, although they inhibited tumor growth. Since the *E1B 55-kDa* sequence is thought to play a crucial role in adenovirus replication, the oncolytic effect of the adenovirus Ad-*MK600* might be related to overexpression of E1B 55-kDa protein. The present findings suggest that Ad-*MK600* has a significantly enhanced therapeutic window for malignant glioma. It has been reported that there is synergy between CRAd (Ad5-Delta24RGD, ONYX-015) and radiotherapy in glioma xenograft models (15,16). Consequently, adjuvant conventional therapy in combination with Ad-*MK* might enhance the oncolytic effect of Ad-*MK* for the treatment of malignant glioma.

Acknowledgements

This study was supported by INCS, Ehime University. We thank Keizo Oka for help in preparing culture medium.

References

1. Surawicz TS, Davis F, Freels S, Laws ER Jr and Menck HR: Brain tumor survival: results from the National Cancer Data Base. J Neurooncol 40: 151-160, 1998.
2. Dirven C, Van Beusechem V, Lamfers M, Grill J, Gerritsen W and Vandertop W: Oncolytic adenoviruses for treatment of brain tumours. Expert Opin Biol Ther 2: 943-952, 2002.
3. Kruyt FA and Curiel DT: Toward a new generation of conditionally replicating adenoviruses: pairing tumor selectivity with maximal oncolysis. Hum Gene Ther 13: 485-495, 2002.
4. Tsutsui J, Kadomatsu K, Matsubara S, Nakagawara A, Hamanoue M, Takao S, Shimazu H, Ohi Y and Muramatsu T: A new family of heparin-binding growth/differentiation factors: increased midkine expression in Wilms' tumor and other human carcinomas. Cancer Res 53: 1281-1285, 1993.
5. Muramatsu H and Muramatsu T: Purification of recombinant midkine and examination of its biological activities: functional comparison of new heparin binding factors. Biochem Biophys Res Commun 177: 652-658, 1991.
6. Ikematsu S, Yano A, Aridome K, Kikuchi M, Kumai H, Nagano H, Okamoto K, Oda M, Sakuma S, Aikou T, Muramatsu H, Kadomatsu K and Muramatsu T: Serum midkine levels are increased in patients with various types of carcinomas. Br J Cancer 83: 701-706, 2000.
7. Mishima K, Asai A, Kadomatsu K, Ino Y, Nomura K, Narita Y, Muramatsu T and Kirino T: Increased expression of midkine during the progression of human astrocytomas. Neurosci Lett 233: 29-32, 1997.
8. Hamada K, Sakaue M, Alemany R, Zhang WW, Horio Y, Roth JA and Mitchell MF: Adenovirus-mediated transfer of HPV 16 E6/E7 antisense RNA to human cervical cancer cells. Gynecol Oncol 63: 219-227, 1996.
9. Hamada K, Kohno S, Iwamoto M, Yokota H, Okada M, Tagawa M, Hirose S, Yamasaki K, Shirakata Y, Hashimoto K and Ito M: Identification of the human IAI.3B promoter element and its use in the construction of a replication-selective adenovirus for ovarian cancer therapy. Cancer Res 63: 2506-2512, 2003.
10. Shono T, Tofilon PJ, Bruner JM, Owolabi O and Lang FF: Cyclooxygenase-2 expression in human gliomas: prognostic significance and molecular correlations. Cancer Res 61: 4375-4381, 2001.
11. Adachi Y, Reynolds PN, Yamamoto M, Wang M, Takayama K, Matsubara S, Muramatsu T and Curiel DT: A midkine promoter-based conditionally replicative adenovirus for treatment of pediatric solid tumors and bone marrow tumor purging. Cancer Res 61: 7882-7888, 2001.
12. Yoshida Y, Tomizawa M, Bahar R, Miyauchi M, Yamaguchi T, Saisho H, Kadomatsu K, Muramatsu T, Matsubara S, Sakiyama S and Tagawa M: A promoter region of midkine gene can activate transcription of an exogenous suicide gene in human pancreatic cancer. Anticancer Res 22: 117-120, 2002.
13. Geoerger B, Grill J, Opolon P, Morizet J, Aubert G, Terrier-Lacombe MJ, Bressac DB, Barrois M, Feunteun J, Kirn DH and Vassal G: Oncolytic activity of the E1B-55 kDa-deleted adenovirus ONYX-015 is independent of cellular p53 status in human malignant glioma xenografts. Cancer Res 62: 764-772, 2002.
14. Nanda D, Vogels R, Havenga M, Avezaat CJ, Bout A and Smitt PS: Treatment of malignant gliomas with a replicating adenoviral vector expressing herpes simplex virus-thymidine kinase. Cancer Res 61: 8743-8750, 2001.
15. Lamfers ML, Grill J, Dirven CM, Van Beusechem VW, Geoerger B, Van DBJ, Alemany R, Fueyo J, Curiel DT, Vassal G, Pinedo HM, Vandertop WP and Gerritsen WR: Potential of the conditionally replicative adenovirus Ad5-Delta24RGD in the treatment of malignant gliomas and its enhanced effect with radiotherapy. Cancer Res 62: 5736-5742, 2002.
16. Geoerger B, Grill J, Opolon P, Morizet J, Aubert G, Lecluse Y, Van Beusechem VW, Gerritsen WR, Kirn DH and Vassal G: Potentiation of radiation therapy by the oncolytic adenovirus dl1520 (ONYX-015) in human malignant glioma xenografts. Br J Cancer 89: 577-584, 2003.

頭蓋内胚細胞性腫瘍おける増殖因子受容体 c-Met 発現の検討

三島 一彦*1 西川 亮*1 廣瀬 隆則*2 松谷 雅生*1

*1埼玉医科大学病院 脳神経外科、*2同 病理学教室1

はじめに

頭蓋内 Germ cell tumors (GCTs) は稀な腫瘍であり、様々な組織形態を示す腫瘍群の総称で、手術および放射線・化学療法による治療成績の違いにより、予後良行群の germinoma, teratoma、中間群の immature teratoma, germinoma with syncytiotrophoblastic giant cells (STGC)、予後不良群の embryonal carcinoma, yolk sac tumor, choriocarcinoma, 及びこれらの混合腫瘍、の3群に大別さる[1]。Germinoma は放射線、化学用法に対する感受性が極めて高く、5年生存率は95%に達するが、予後不良群に属する GCTs では手術、放射線、化学療法による治療にも拘わらず、5年生存率は20%以下である[1]。従って、GCTs の腫瘍組織型を分類することは治療法の選択を決定するうえで重要であり、組織の鑑別に有用な腫瘍マーカーの存在は不可欠であると考えられる。C-kit はレセプター型チロシンキナーゼであり、germ cell の生存や分化に重要な役割を果たしていることがこれまでの研究により示されている[2]。また、精巣 GCTs での発現が検討され、seminoma では高い発現を認め、腫瘍形成に関与していることが示唆されている[3]。さらに頭蓋内 germinoma での発現も、精巣腫瘍同様に認められ、その分泌型である s-kit は腫瘍マーカーとして診断に役立つことが期待されている[4]。一方、中間群、予後不良群に属する組織型では c-kit の発現は認められず[3),4]、c-kit system 以外のレセプター型チロシンキナーゼが腫瘍化に関与している可能性があると考えられる。Hepatocyte growth factor (HGF) のレセプターである c-Met は、これまで種々の癌腫で発現が亢進し、腫瘍の増大、浸潤、転移などを促進すること、また予後と相関していることが報告されている[5]。さらに c-Met は、胚細胞の分化や、胎盤の形成に重要な役割を果たしていることが示されていることより[6),7]、我々は頭蓋内 GCTs の手術摘出標本を用い、c-Met の発現を検討した。

1．対象と方法

免疫組織化学染色

当院で手術された GCTs 26例（germinoma 12例、mixed germ cell tumor で主に teratoma のもの2例、germinoma with STGC 2例、immature teratoma 3例、mixed GCTs の構成組織が主に embryonal carcinoma のもの3例、主に yolk sac tumor のもの2例、choriocarcinoma 2例）を用いた。Informed consent を得た上で、一部の症例では腫瘍摘出後、ただちに凍結した腫瘍をたんぱく抽出に使用した。腫瘍組織はホルマリン固定後パラフィン包埋切片を作成した。0.01M クエン酸（pH 6.0）によるマイクロウエーブ処理後、1次抗体として、抗ヒト c-kit 抗体（Dako)、抗ヒト c-Met 抗体（C-28, Santa Cruz)、Phospho-Met (Tyr1349, Tyr1234/1235) 抗体（Cell Signaling Technology)を使用し、ABC法で免疫組織化学染色を行った。

免疫沈降・ウェスタンブロット法

腫瘍組織よりたんぱくを抽出し定量後、抗ヒト c-Met 抗体と protein A-Sepharose beads を加え免疫複合体を形成させ、wash buffer で洗浄後、7.5% SDS-ポリアクリルアミドゲルに電気泳動、ニトロセルロース膜に転写し、1次抗体、2次抗体と反応、洗浄後 ECL キット (Amersham) で検出した。

2．結　果

1）GCTs における c-Met 発現の免疫組織化学的検討 (Table 1, Figure 1)

Table 1 に腫瘍組織型と c-Met の染色結果を示す。また、Fig. 1 には、各組織型における c-Met, c-kit の代表的な免疫組織染色例を提示する。C-Met は germinoma では12例中9例で陰性で、残る3例ではごく一部の腫瘍細胞の細胞質が非常に淡く陽性を示すのみであった（Fig. 1A)。一方、c-kit 抗体では germinoma 全例で腫瘍細胞膜が強く染色された (B)。Germinoma with STGC では2例中2例で STGC が c-Met 強陽性を示すほか、一部の腫瘍細胞も陽性を示した（C）が、C-kit は germinoma 細胞成分のみ陽性であった（D)。Immature teratoma では3例いずれも、未熟な腺上皮細胞膜に c-Met の発現が強く認められたが（E)、C-kit は陰性であった（F)。Embryonal carcinoma では3例すべてで、多層性管状に増殖した上皮様腫瘍細胞膜に c-Met の強い陽性所見が認められ、間質細胞は陰性であった（G)。Yolk sac tumor では2例中2例で、網目状に配列する腫瘍細胞が陽性であり（I)、choriocarcinoma では2例いずれも、syncytiotrophoblastic cell, cytotrophoblas-

Table 1. Expression of c-Met and c-kit in intracranial germ cell tumors

Prognosis	Histology	C-Met +	C-Kit +
Good	Germinoma	±3/12 (−9/12)	12/12
	Teratoma	1/2 (±1/2)	1/2 (−1/2)
Intermediate	Germinoma with STGC	2/2	2/2
	Immature teratoma	3/3	0/3
Poor	Embryonal carcinoma	3/3	0/3
	Yolk sac tumor	2/2	0/2
	Choriocarcinoma	2/2	0/2

tic cell 共に主に細胞膜を中心に c-Met 陽性を示した(K)。C-kit はこれらの予後不良群 GCTs でいずれにおいても陰性であった (H, J, L)。

2) C-Met リン酸化状態の検討

Phospho-Met 抗体を用いた免疫染色法で腫瘍組織中の c-Met の活性化を検討した。C-Met の発現があった embryonal carcinoma では一部の上皮様腫瘍細胞の細胞膜に phospho-Met の陽性所見を認めた(Figure 1-M)。

3) C-Met 発現レベルの検討 (Figure 2)

GCTs 腫瘍組織よりタンパクを抽出し、c-Met の発現を免疫沈降・ウェスタンブロット法にて確認した。Germinoma では発現がみられず、embryonal carcinoma, yolk sac tumor では c-Met が高発現していることが確認された。

3. 考 察

増殖因子／レセプターの質的、量的な発現異常は、その下流のシグナル伝達系の活性化をもたらし、腫瘍細胞の増殖、分化、細胞死の抑制、血管新生などを介し腫瘍形成、進展、浸潤、転移などに深く関わると考えられている。GCTs における増殖因子／レセプターの発現を検討した研究は少なく、特に頭蓋内 GCTs においてはほとんど研究されていないのが現状である。精巣 GCTs においてこれまで報告されているものとして、fibroblast growth factor (FGF) のメンバーである HST-1 や FGF4, 8、FGF receptor 1 が主に non-seminomatous GCTs に発現していること[8]、c-kit が seminoma に発現し[9]、c-kit の変異活性型が約 25%で発現していること[10]、血管新生に関わる VEGF の発現が GCTs で高いこと、EGFR が choriocarcinoma の syncytiotrophoblastic cell で発現し、TGFαとオートクラインループを形成し、腫瘍細胞の増殖に関わる可能性があること[11]、動物モデルでは GDNF のトランスジェニックマウスで seminoma が発生することが示されている[12]。しかし、これまでに GCTs 組織において c-Met の発現及び機能を調べた報告はない。C-Met／HGF は種々の癌で、発現亢進がみられ、オートクラインあるいはパラクラインループを形成し、腫瘍細胞の増殖、遊走促進による浸潤、転移、血管新生などに関与し、悪性度や予後とも相関することが知られている[5]。また、c-Met を高発現させると HGF の関与なくとも腫瘍細胞運動能が亢進する[13]。C-Met は胎盤では trophoblasts に発現しており[7]、*in vitro* で cytotrophoblast の増殖や浸潤に関与していることが示されている[14]。また、最近、choriocarcinoma 細胞株において c-Met は恒常的に活性化されていることが示された[15]。今回の我々の検討でも、choriocarcinoma の腫瘍細胞で c-Met の強い発現がみられたことから、c-Met は腫瘍細胞の増殖や浸潤に関係している可能性がある。EGFR からのシグナル伝達系が活性化されると c-Met の発現、活性化がおこることが甲状腺癌細胞などで示されており[16]、choriocarcinoma では TGFα／EGFR システムが活性化している[11]ことから、EGFR からのシグナルが c-Met の発現を亢進させている可能性がある。

C-Met は癌化だけでなく、胎児発生期の組織分化や形態形成にも関わっている[17]。P19 マウス embryonal carcinoma 細胞株は、retinoic acid 添加で neuroectodermal に、DMSO 添加で mesodermal 細胞に分化するため、*in vitro* のモデルとして頻用される。この系では、c-Met は分化とともに発現とそのリン酸化の増強が起る[18]。また、c-Met は胎児形成発達の際、管腔構造誘導にも関わっており、我々の免疫組織染色の検討で、embryonal carcinoma や、immature teratoma では、分化傾向を示す腺管を形成した上皮細胞に発現が高く見られたことは、これらの腫瘍細胞での分化や腺管形成に

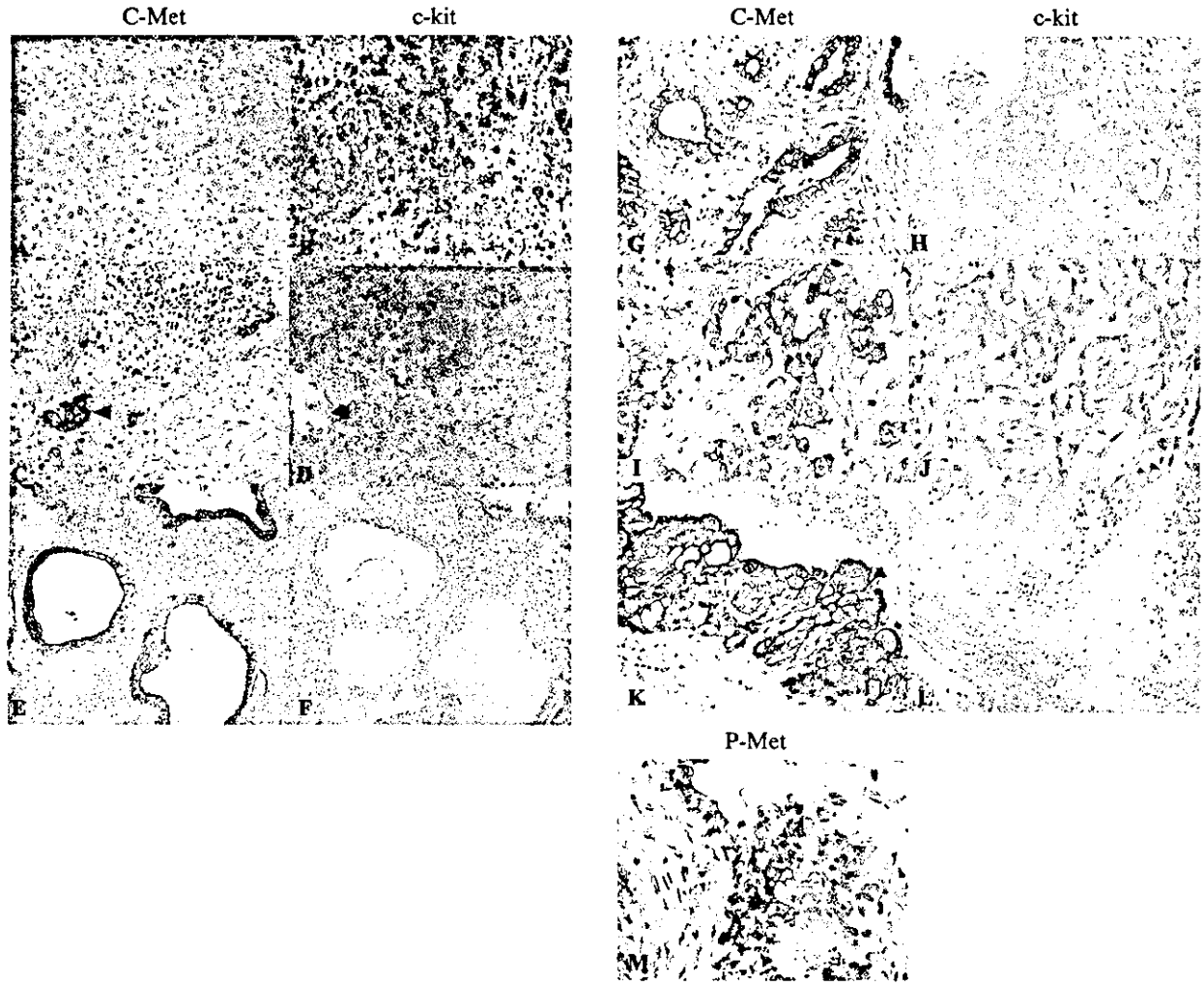

Figure 1. Immunohistochemical findings in different intracranial germ cell tumors
A. B. Germinoma. Tumor cells were negative for c-Met (A) and positive for c-kit (B). X200
C. D. Germinoma with STGC. Syncytiotrophoblastic giant cells (arrow heads) and surrounding tumor cells were positive for c-Met (C). Syncytiotrophoblastic giant cells were negative for c-kit (D). X200
E. F. Immature teratoma. Immunoreactivity for c-Met showed positive in tumor cells displaying epitherial differentiation. C-Met was negative in the mesenchymal component (E). Immunoreactivity for c-kit was not detected in any components (F). X100
G. H. Embryonal carcinoma. C-Met was strongly expressed on the cell surface of the epithelial tumor cells (G). Immunoreactivity for c-Kit was not detected in any components (H). X200
I. J. Yolk sac tumor. C-met was strongly expressed on the tumor cell surface membrane (I). Tumor cells displayed negative reaction for c-kit (J). X200
K. L. Choriocarcinoma. The membrane and cytoplasm of both syncytiotrophoblastic giant cells and cytotrophoblasts were strongly positive for c-Met (K). Tumor cells displayed negative reaction for c-kit (L). X200
M. Phospho-c-Met expression. The membrane expression of the activated form of c-Met (phosphorylated c-Met) was detected in c-Met-positive embryonal carcinoma. X200

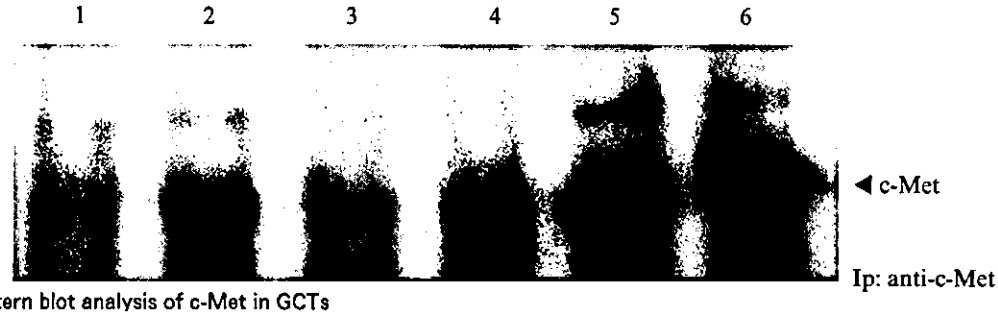

Figure 2. Western blot analysis of c-Met in GCTs
The Met protein was highly expressed in the yolk sac tumors (lanes 2-4) and embryonal carcinomas (lanes 5, 6), but not expressed in germinoma (lane 1).

関与している可能性があると考えられる。今回のリン酸化c-Metに対する抗体を用いた検討で、c-Metの発現が高いembryonal carcinomaではc-Metが活性化されている可能性が示唆されたが、c-MetのGCTsにおける機能をさらに解析するためには、頭蓋内GCTsから腫瘍細胞株を樹立し、*in vitro*での解析をすすめる必要があろう。

前述のように、C-kit/SCFはprimordial germ cellの遊走や生存に関係しており、c-kitの発現亢進が精巣seminomaで認められている[3]。今回の我々の検討でもc-kitは頭蓋内germinomaに発現が確認された。リンパ球や組織球が主体をなす肉芽腫様変化の強いgerminomaでは診断に苦慮することがあり、腫瘍細胞を検出し、確定診断をくだすのにc-kitは有用であると考えられる。一方、臨床的には、GCTsの腫瘍組織内にnon-germinomaの成分を見つけだすことは、治療法の選択、予後を知る上で重要である。C-Metは、我々の検討では予後不良群、中間群に属する腫瘍組織に高い発現が認められ、これらの組織型の検出のためのマーカーの1つとなる可能性がある。

近年、チロシンキナーゼ阻害剤を用いた分子標的治療法が開発され、c-kitを標的としたSTI571の臨床試験が悪性gastrointestinal stromal tumorや化学療法抵抗性の転移性seminomaで行われている[10]。C-Metのチロシンキナーゼ阻害薬であるK252aやSU11271を用いた治療法の開発も進められており[5),19)]、今後頭蓋内germinomaに対するc-kit、non-germinomatous GCTsに対するc-Metを標的とした治療応用の可能性があると考えられる。

結　語

C-Metはc-kitと異なり、予後の不良なGCTsにおいて高発現しており、GCTsの悪性化や腫瘍組織の形態形成に関与している可能性が示唆された。c-Metはnon-germinomatous GCTsの新たな腫瘍マーカーとなる可能性があると考えられた。

参考文献

1) Matsutani M. Japanese Pediatric Brain Tumor Study Group. Combined chemotherapy and radiation therapy for CNS germ cell tumors--the Japanese experience. J Neurooncol. 2001; 54: 311-316.

2) Mauduit C, Hamamah S, Benahmed M. Stem cell factor/c-kit system in spermatogenesis. Hum Reprod Update. 1999; 5: 535-545

3) Devouassoux-Shisheboran M, Mauduit C, Tabone E, Droz JP, Benahmed M. Growth regulatory factors and signalling proteins in testicular germ cell tumours. APMIS. 2003; 111: 212-224

4) Miyanohara O, Takeshima H, Kaji M, Hirano H, Sawamura Y, Kochi M, Kuratsu J. Diagnostic significance of soluble c-kit in the cerebrospinal fluid of patients with germ cell tumors. J Neurosurg. 2002; 97: 177-183

5) Haddad R, Lipson KE, Webb CP. Hepatocyte growth factor expression in human cancer and therapy with specific inhibitors. Anticancer Res. 2001; 21: 4243-4252

6) Depuydt CE, Zalata A, de Potter CR, van Emmelo J, Comhaire FH. The receptor encoded by the human C-MET oncogene is expressed in testicular tissue and on human spermatozoa. Mol Hum Reprod. 1996; 2: 2-8

7) Somerset DA, Li XF, Afford S, Strain AJ, Ahmed A, Sangha RK, Whittle MJ, Kilby MD. Ontogeny of hepatocyte growth factor (HGF) and its receptor (c-met) in human placenta: reduced HGF expression in intrauterine growth restriction. Am J Pathol. 1998; 153: 1139-1147

8) Suzuki K, Tokue A, Kamiakito T, Kuriki K, Saito K, Tanaka A. Predominant expression of fibroblast growth factor (FGF) 8, FGF4, and FGF receptor 1 in nonseminomatous and highly proliferative components of testicular germ cell tumors. Virchows Arch. 2001; 439: 616-621

9) Strohmeyer T, Reese D, Press M, Ackermann R, Hartmann M, Slamon D. Expression of the c-kit proto-oncogene and its ligand stem cell factor (SCF) in normal and malignant human testicular tissue. J Urol. 1995; 153: 511-5

10) Kemmer K, Corless CL, Fletcher JA, McGreevey L, Haley A, Griffith D, Cummings OW, Wait C, Town A, Heinrich MC. KIT mutations are common in testicular seminomas. Am J Pathol. 2004; 164: 305-313

11) Moroni M, Veronese S, Schiavo R, Carminati O, Sorensen BS, Gambacorta M, Siena S. Epidermal growth factor receptor expression and activation in nonseminomatous germ cell tumors. Clin Cancer Res. 2001; 7: 2770-5

12) Meng X, de Rooij DG, Westerdahl K, Saarma M, Sariola H. Promotion of seminomatous tumors by targeted overexpression of glial cell line-derived neurotrophic factor in mouse testis. Cancer Res. 2001; 61: 3267-3271

13) Nakamura T, Kanda S, Yamamoto K, Kohno T, Maeda K, Matsuyama T, Kanetake H. Increase in hepatocyte growth factor receptor tyrosine kinase activity in renal carcinoma cells is associated with increased motility partly through phosphoinositide

3-kinase activation. Oncogene. 2001; 20:7610-7623
14) Saito S, Sakakura S, Enomoto M, Ichijo M, Matsumoto K, Nakamura T. Hepatocyte growth factor promotes the growth of cytotrophoblasts by the paracrine mechanism. J Biochem (Tokyo). 1995; 117: 671-6
15) Takayanagi T, Aoki Y, Tanaka K. Expression of constitutively active c-MET receptor in human choriocarcinoma. Gynecol Obstet Invest. 2000; 50: 198-202
16) Bergstrom JD, Westermark B, Heldin NE. Epidermal growth factor receptor signaling activates met in human anaplastic thyroid carcinoma cells. Exp Cell Res. 2000; 259: 293-9
17) Kolatsi-Joannou M, Moore R, Winyard PJ, Woolf AS. Expression of hepatocyte growth factor/scatter factor and its receptor, MET, suggests roles in human embryonic organogenesis. Pediatr Res. 1997; 41: 657-665
18) Yang XM, Park M. Expression of the met/hepatocyte growth factor/scatter factor receptor and its ligand during differentiation of murine P19 embryonal carcinoma cells. Dev Biol. 1993; 157: 308-320.
19) Wang X, Le P, Liang C, Chan J, Kiewlich D, Miller T, Harris D, Sun L, Rice A, Vasile S, Blake RA, Howlett AR, Patel N, McMahon G, Lipson KE. Potent and selective inhibitors of the Met [hepatocyte growth factor/scatter factor (HGF/SF) receptor] tyrosine kinase block HGF/SF-induced tumor cell growth and invasion. Mol Cancer Ther. 2003; 2: 1085-1092

Brain Tumor Pathol (2004) 21:53–56
DOI 10.1007/s10014-004-0154-1

SPECIAL ARTICLE

Ryo Nishikawa · Tatsuya Sugiyama · Yoshitaka Narita
Frank Furnari · Webster K. Cavenee · Masao Matsutani

Immunohistochemical analysis of the mutant epidermal growth factor, ΔEGFR, in glioblastoma

Received and accepted: February 5, 2004

Abstract The naturally occurring mutated form of the epidermal growth factor receptor, ΔEGFR (also named EGFRvIII and de2-7EGFR), greatly enhances glioblastoma (GBM) cell growth in vivo through several activities, such as down-regulating p27 and up-regulating BclX(L) while increasing signaling through the RAS-MAPK and PI3-K cascades. More than half of GBMs, especially of the de novo type, overexpress EGFR, and 50%–70% of these express ΔEGFR. However, little is known about the distribution of ΔEGFR-expressing tumor cells within surgical specimens. In order to address this clinically important issue, we performed immunohistochemical analyses of 53 GBMs obtained during surgery using the anti- ΔEGFR monoclonal antibody, DH8.3. We also simultaneously analyzed wild-type EGFR expression in these tissues using the anti-EGFR monoclonal antibody, EGFR.113. ΔEGFR and wild-type EGFR expression were observed in 20/53 (38%) and 29/53 (55%), respectively. Nineteen (95%) of the ΔEGFR-positive tumors also expressed wild-type EGFR; one case was ΔEGFR-positive but wild-type EGFR-negative. In 13/20 (65%) of the ΔEGFR-positive tumors, tumor cells were scattered diffusely within the tumors, 6/20 showed geographical distribution of ΔEGFR-positive tumor cells, and one case showed homogeneous staining. In the wild-type EGFR-positive cases, almost all tumor cells expressed EGFR. The differential distribution of cells expressing the two receptors observed here may suggest either that ΔEGFR arises at a low frequency from wild-type EGFR-expressing cells, perhaps during the process of gene amplification, or that there is a paracrine-type of interaction between them.

Key words Epidermal growth factor receptor · Glioblastoma · Immunohistochemistry

R. Nishikawa (✉) · T. Sugiyama · M. Matsutani
Department of Neurosurgery, Saitama Medical School, 38 Morohongo, Moroyama-machi, Iruma-gun, Saitama 350-0495, Japan
Tel. +81-49-276-1334; Fax +81-49-294-4955
e-mail: rnishika@saitama-med.ac.jp

Y. Narita · F. Furnari · W.K. Cavenee
Ludwig Institute for Cancer Research, San Diego, CA, USA

W.K. Cavenee
Department of Medicine, Center for Molecular Genetics and Cancer Center, University of California at San Diego, La Jolla, CA, USA

Indroduction

The epidermal growth factor receptor (EGFR) gene is amplified at the DNA level and overexpressed at the level of mRNA or protein expression in tumor tissues of about 40%–50% of human glioblastoma (GBM) cases.[1–3] This EGFR gene amplification is often followed or accompanied by further gene rearrangement. About two-thirds of such rearrangements result in a particular mutant form called-ΔEGFR, de2-7EGFR, or EGFRvIII, an in-frame deletion of exons 2–7 resulting in a deletion of 267 amino acids.[4–6] The resulting mutant protein is ligand independent, constitutively phosphorylated, and localized primarily to the cell surface.[7–9] ΔEGFR promotes the tumorigenesis of GBM cells in vivo by increasing cellular proliferation,[10] decreasing cellular apoptosis,[11] and promoting tumor cell invasion.[12] However, these conclusions have derived from the analysis of the behavior of xenografts that arose after inoculation of cells expressing relatively homogeneous levels of ΔEGFR, and little is known about the distribution of ΔEGFR-expressing tumor cells in surgical specimens. Since this limits understanding of the clinical significance of ΔEGFR, we performed immunohistochemical analysis of ΔEGFR and wild-type EGFR expression in primary GBM tissues. Our results revealed differential distribution of tumor cells expressing these receptors, suggesting potential interactions between them.

Materials and methods

Brain tumor samples

Fifty-three GBM specimens that were surgically resected between 1989 and 2002 at Saitama Medical School were subjected to investigation. All tumors were diagnosed according to the World Health Organization (WHO) classification of brain tumors.[13] Tissue samples were fixed in 10% formalin and embedded in paraffin for histological as well as immunohistochemical examination. For Western blotting, samples were snap-frozen in liquid nitrogen in the operating rooms and stored at −80°C until use. Twenty samples were available for this series of studies.

Immunohistochemistry

The sections were deparaffinized, rehydrated, and incubated in hydrogen peroxide to block endogenous peroxidase activity, followed by antigen retrieval in a steam cooker and preincubation in normal goat serum. An anti-ΔEGFR monoclonal antibody, DH8.3, raised against a synthetic peptide spanning the unique junctional sequence of the deleted part of ΔEGFR,[14] was diluted 1:50 and applied to the samples for 1 h at room temperature. DH8.3 does not react with wild-type EGFR.[14] A standard ABC method was performed according to the manufacturer's recommendations (Vectastain, Vector Laboratories, Burlingame, CA, USA), and diaminobenzidine tetrahydrochloride was used to visualize the immunoreactivities. The slides were lightly counterstained with hematoxylin. Anti-EGFR monoclonal antibody, EGFR.113, raised against the extracellular domain of the wild-type EGFR was purchased from Novocastra (Newcastle, UK) and used for immunohistochemistry according to the manufacturer's recommendations.

Western blotting

The tissue specimens were lysed in extraction buffer (50 mM Tris-HCl [pH 7.6], 50 mM NaCl, 2% NP-40, 0.5% deoxycholic acid, 0.2% sodium dodecyl sulfate [SDS], 1 mM phenylmethylsulfonyl fluoride, 5 μg/ml leupeptin, 5 μg/ml aprotinin, and 0.5 mM Na_3VO_4) and sonicated. The lysates were centrifuged at 8000*g* for 5 min, and the supernatants were collected. Each protein sample (20 μg) was separated with 7.5% polyacrylamide/SDS gels and electroblotted onto nitrocellulose membranes (ECL membrane, Amersham Pharmacia Biotech, Piscataway, NJ, USA). After blocking with 5% skim milk in Tris-buffered saline with 0.05% Tween 20, the membranes were incubated with an anti-EGFR monoclonal antibody, C13, which reacts with both wild-type EGFR and ΔEGFR (a kind gift from Dr. Gordon Gill, University of California at San Diego), and then incubated with a horseradish peroxidase-conjugated antimouse secondary antibody (Vector Laboratories), and subjected to chemiluminescence detection (ECL, Amersham Pharmacia Biotech).

Image intensification

The images from immunohistochemistry and Western blotting were captured with a digital camera and processed with Adobe Photoshop 7.0 on an Apple Macintosh computer.

Results

Immunohistochemistry

Positive immunoreactivities for DH 8.3 and EGFR.113 were observed in 20/53 (38%) and 29/53 (55%), respectively. Of those 20 cases positive for DH8.3, 19 were also positive and 1 was negative for EGFR.113. Typical examples of DH8.3-immunoreactivity are shown in Fig. 1A–E. Immunoreactivities for DH8.3 were observed on the cell membrane or in the cytoplasm of tumor cells that were similar to those for EGFR.113 (Fig. 1A and F). Immunoreactive cells were scattered diffusely in the 13 of 20 (65%) specimens positive for DH8.3 (Fig. 1A and B). In six specimens (30%), cells immunoreactive for DH8.3 were geographically distributed (Fig. 1C). The remaining specimen showed a homogeneous distribution of immunoreactive cells. In one specimen, DH8.3-immunoreactive cells were observed adhering to tumor vessels (Fig. 1D and E). On the other hand, in the tumors immunoreactive for EGFR.113, almost all tumor cells had homogeneous immunoreactivities, as shown in Fig. 1F, except for one case that showed geographical distribution of EGFR-expressing cells. Figure 1F is from the same area of the same specimen shown in Fig. 1B.

Western blotting

Significant amounts of ΔEGFR and full-length EGFR were detected in 9 of 20 (45%; lanes 5, 6, 8, 9, 10, 11, 13, 17, and 20 in Fig. 2) and 12 of 20 (60%, lanes 2, 5, 6, 7, 8, 9, 10, 11, 13, 15, 17, and 20 in Fig. 2) samples by Western blotting, respectively. Three samples (lanes 2, 11, and 15 in Fig. 2) were negative for EGFR.113 by immunohistochemistry but positive for full-length EGFR by Western blotting. None of the samples negative for full-length EGFR by Western blotting was positive for EGFR.113 by immunohistochemistry, and both results were concordant in 17/20 (85%) of the samples. Four samples (lanes 5, 9, 11, and 17 in Fig. 2) were negative for DH8.3 by immunohistochemistry and positive for ΔEGFR by Western blotting, and both results were concordant in 16/20 (80%).

Discussion

Expression of ΔEGFR was observed in 20/53 (38%) of GBM samples by immunohistochemistry and 9/20 (45%) by Western blotting. Those frequencies were similar to those

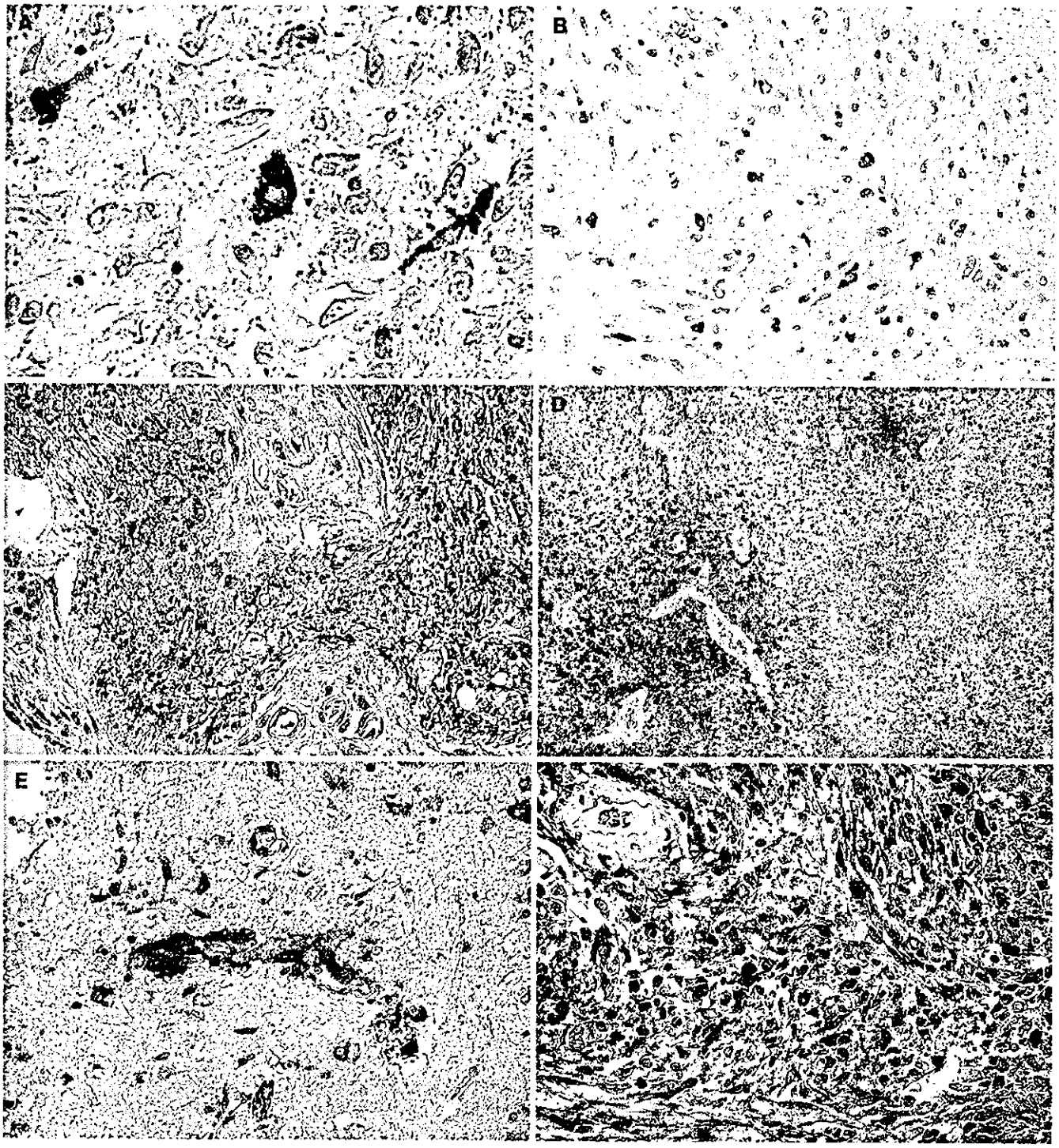

Fig. 1. Immunohistochemical detection of mutated epidermal growth factor receptor (ΔEGFR) (**A–E**) and wild-type EGFR (**F**) expression in glioblastoma specimens. Original magnifications are (**A**) ×1000, (**B, C, E, F**) ×400, and (**D**) ×100

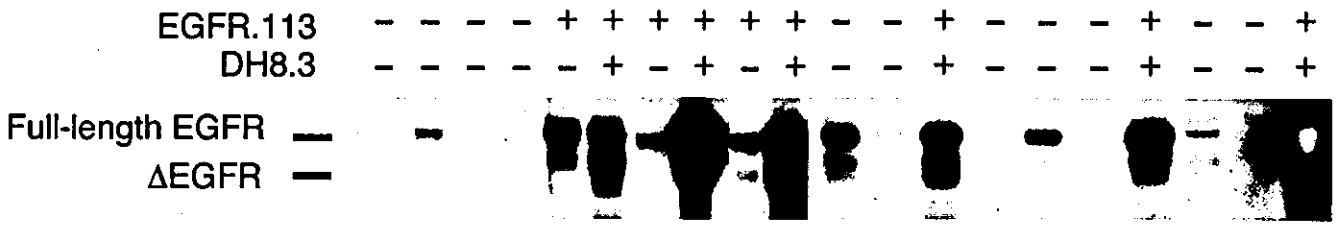

Fig. 2. Western blotting analysis of *ΔEGFR* and wild-type *EGFR* expression in glioblastoma specimens. + or − indicates immunoreactivities for *DH8.3* and *EGFR.113* by immunohistochemistry

in reported series: 7/12 (58%) by Western blotting,[5] and 8/12 (67%)[5] or 12/21 (62%)[4] by immunohistochemistry. Among the 20 cases in which frozen samples were available for Western blotting, the results of Western blotting and immunohistochemistry were concordant in 16 cases (80%). Expression of ΔEGFR in the remaining four cases was positive by Western blotting but negative by immunohistochemistry, which would indicate either that Western blotting was more sensitive for the detection of low levels of ΔEGFR expression, or that there were sampling errors due to the heterogeneous location of positive cells.

Each of the 20 cases that were immunoreactive for DH8.3 by immunohistochemistry was also immunoreactive for EGFR.113, with one exception. Among the 29 cases positive for EGFR.113, 19 (66%) were positive for DH8.3. It has been reported that GBMs with ΔEGFR mutation always harbor increased *EGFR* gene dosage, and frequency of ΔEGFR found in GBMs with *EGFR* amplification was 67%.[6] These data suggest that amplification of the *EGFR* gene precedes *EGFR* mutation.

GBM cells expressing ΔEGFR have a remarkable in vivo growth advantage.[7] One consequence of this could be a clonal expansion of the cell population. Consonant with this notion are reported experiments showing that injection of a mixture of U87MG.ΔEGFR (a GBM cell line expressing ΔEGFR) and parental U87MG at a 1:50000 ratio into nude mouse brains showed an outgrowth of U87MG.ΔEGFR cells, with the proportion reaching 83% in the tumors that developed.[11] The geographical distribution of ΔEGFR-expressing tumor cells observed in surgical specimens has been believed to be the result of an analogous clonal expansion. However, our results here show that GBM tumor cells expressing ΔEGFR prefer to distribute diffusely in a scattering pattern in the majority of cases. In contrast, tumor cells expressing wild-type EGFR appeared to distribute in a more homogeneous fashion (Fig. 1F). The differential distribution of ΔEGFR- and wild-type EGFR-expressing tumor cells, together with the fact that almost all tumors expressing ΔEGFR expressed wild-type EGFR, appears to support the hypothesis that ΔEGFR arises at a low frequency from wild-type EGFR-expressing cells. The significantly enhanced biological aggressiveness of the tumor cells expressing ΔEGFR, together with their often diffuse occurrence among other tumor cells, also raises the possibility that they might provide a positive field effect on surrounding tumor cells that overexpress wild-type EGFR. The nature of such interactions requires further study.

Acknowledgments We thank Ms. Naoko Teshima for her excellent technical assistance. This work was supported in part by grants from the National Cancer Institute, NIH and the National Foundation for Cancer Research (both to WKC).

References

1. Wong AJ, Bigner SH, Bigner DD, et al (1987) Increased expression of the epidermal growth factor receptor gene in malignant gliomas is invariably associated with gene amplification. Proc Natl Acad Sci USA 84:6899–6903
2. Ekstrand AJ, Sugawa N, James CD, et al (1992) Amplified and rearranged epidermal-growth-factor-receptor genes in human glioblastomas reveal deletions of sequences encoding portions of the N- and/or C-terminal tails. Proc Natl Acad Sci USA 89:4309–4313
3. Simmons ML, Lamborn KR, Takahashi M, et al (2001) Analysis of complex relationships between age, p53, epidermal growth factor receptor, and survival in glioblastoma patients. cancer Res 61:1122–1128
4. Wikstrand CJ, Hale LP, Batra SK, et al (1995) Monoclonal antibodies against EGFRvIII are tumor specific and react with breast and lung carcinoma and malignant gliomas. Cancer Res 55:3140–3148
5. Feldkamp MM, Lala P, Lau N, et al (1999) Expression of activated epidermal growth factor receptors, Ras-guanosine triphosphate, and mitogen-activated protein kinase in human glioblastoma multiforme specimens. Neurosurgery 45:1441–1453
6. Frederick L, Wang X-Y, Eley G, et al (2000) Diversity and frequency of epidermal growth factor receptor mutations in human glioblastomas. Cancer Res 60:1383–1387
7. Nishikawa R, Ji XD, Harmon RC, et al (1994) A mutant epidermal growth factor receptor common in human glioma confers enhanced tumorigenicity. Proc Natl Acad Sci USA 91:7727–7731
8. Huang H-JS, Nagane M, Klingbeil CK, et al (1997) The enhanced tumorigenic activity of a mutant epidermal growth factor receptor common in human cancers is mediated by threshold levels of constitutive tyrosine phosphorylation and unattenuated signaling. J. Biol Chem 272:2027–2935
9. Wikstrand CJ, McLendon RE, Friedman AH, et al (1997) Cell surface localization and density of the tumor-associated variant of the epidermal growth factor receptor, EGFRvIII. Cancer Res 57: 4130–4140
10. Narita Y, Nagane M, Mishima K, et al (2002) Mutant epidermal growth factor receptor signaling down-regulates p27 through activation of the phosphatidylinositol 3-kinase/Akt pathway in glioblastomas. Cancer Res 62:6764–6769
11. Nagane M, Coufal F, Lin H, et al (1996) A common mutant epidermal growth factor receptor confers enhanced tumorigenicity on human glioblastoma cells by increasing proliferation and reducing apoptosis. Cancer Res 56:5079–5086
12. Lal A, Glazer CA, Martinson HM, et al (2002) Mutant epidermal growth factor receptor up-regulates molecular effectors of tumor invasion. Cancer Res 62:3335–3339
13. Kleihues P, Burger PC, Collins VP, et al (2000) Glioblastoma. In: Kleihues P, Cavenee WK (eds) Pathology and genetics of tumours of the nervous system. IARC, Lyon, pp 29–39
14. Hills D, Rowlinson-Busza G, Gullick WJ (1995) Specific targeting of a mutant, activated EGF receptor found in glioblastoma using a monoclonal antibody. Int J Cancer 63:537–543

Int. J. Radiation Oncology Biol. Phys., Vol. 60, No. 1, pp. 214–217, 2004

0360-3016/04/$ see front matter

ELSEVIER

doi:10.1016/j.ijrobp.2004.02.024

CLINICAL INVESTIGATION **Brain**

IMPACT OF MARGIN FOR TARGET VOLUME IN LOW-DOSE INVOLVED FIELD RADIOTHERAPY AFTER INDUCTION CHEMOTHERAPY FOR INTRACRANIAL GERMINOMA

HIROKI SHIRATO, M.D., HIDEFUMI AOYAMA, M.D., JUN IKEDA, M.D., KENJI FUJIEDA, M.D., NORIO KATO, M.D., NOBUAKI ISHII, M.D., KAZUO MIYASAKA, M.D., YOSHINOBU IWASAKI, M.D., AND YUTAKA SAWAMURA, M.D.

Departments of Radiology, Neurosurgery, and Pediatrics, Hokkaido University School of Medicine, Sapporo, Japan

Purpose: We previously published a report stating that germinomas with elevated serum beta human chorionic gonadotropin (HCG-β) had a poor relapse rate, but these findings have not been supported by a multi-institutional trial. The margin for initial gross tumor volume (GTV) before surgery and chemotherapy of the same materials was investigated by retrospective review.

Methods and Material: The 27 patients reported on in the previous paper were analyzed. The two-dimensional margin from the initial GTV to 90% of the prescribed dose of 24 Gy was 2.0 cm for a solitary lesion in the protocol. This margin was measured retrospectively without knowledge of the serum HCG-β level. The whole ventricle field was used for patients with multifocal disease and whole central nervous system field was used for disseminated disease, respectively.

Results: Six relapses were seen in 18 patients with solitary tumors, and were treated with the minimum margin of 1.5 cm or less to the initial GTV. Five of the 6 had initially elevated serum HCG-β at the median of 7.4 mIU/mL, ranging from 0.7–233 mIU/mL. No relapses were seen in the 9 patients who were treated with whole ventricle or whole central nervous system field.

Conclusions: An inadequate margin and elevated serum HCG-β were equally determined to be candidates that caused the poor local control. The whole ventricle is recommended as the smallest target volume for germinoma with or without elevated HCG-β after induction chemotherapy. © 2004 Elsevier Inc.

Germinoma, Central nervous system, Radiotherapy, Induction chemotherapy.

INTRODUCTION

Whole ventricle or larger fields have been the standard of care for intracranial germinoma in our institution (1), as in other institutions (2–4). The possibility of reducing the dose and volume was suggested by the usage of cisplatin-based chemotherapy in the early 1990s (5). A Phase II study on induction cisplatin-based chemotherapy for germinomas followed by 24 Gy radiotherapy was conducted as a regional study in the Hokkaido district of Japan (6). The results of the Phase II study showed a higher relapse rate in germinomas with elevated serum human chorionic gonadotropin beta (HCG-β) than in those without elevated serum HCG-β (7). However, a nationwide prospective study using platinum-based induction chemotherapy followed by low-dose radiotherapy for 130 germinoma patients without elevation of HCG-β, and 34 germinoma patients with elevated HCG-β, did not show significant differences in the relapse-free rate between germinomas without elevated serum HCG-β and germinomas with elevated serum HCG-β (8). Furthermore, treatment volume was reported to be a significant prognostic factor in the nation-wide study. This discrepancy in the significance of HCG-β and the treatment volume prompted us to reevaluate the treatment results of the Hokkaido study by conducting a precise review of the treatment volume.

The purpose of this study is to investigate the impact of margins for the target volume in low-dose involved field radiotherapy after induction chemotherapy for intracranial germinoma.

METHODS AND MATERIALS

The eligibility criteria for patients receiving the induction chemotherapy followed by low-dose radiotehrapy were (*1*) 3 years old or older, (*2*) histologically proven germinoma, and (*3*) no previous chemotherapy or radiotherapy. The patients were classified into two groups as follows: (*1*) a good prognosis group, consisting of patients with a solitary

Reprint requests to: Hiroki Shirato, M.D., Department of Radiology, Hokkaido University School of Medicine, North-15 West-7, Kita-ku, Sapporo 060-8638, Japan. Tel: (+81) 11-706-5975; Fax: (+81) 11-706-7876; E-mail: hshirato@radi.med.hokudai.ac.jp

Received Oct 17, 2003, and in revised form Feb 6, 2004. Accepted for publication Feb 9, 2004.

germinoma with serum HCG-β < 0.5 mIU/mL, which was the normal upper limit in our institute, and (2) an intermediate prognosis group, consisting of patients with a solitary germinoma with HCG-β ≥ 0.5 mIU/mL, a multifocal germinoma (two or more lesions without evidence of dissemination), and disseminated germinoma (cytological or imaging evidence of dissemination). For the good prognosis group, 3–4 cycles of etoposide (100 mg/m^2) and cisplatin (20 mg/m^2) were given for 5 days every 4 weeks. For the intermediate prognosis group, 3–6 cycles of ifosfamide (900 mg/m^2), cisplatin (20 mg/m^2), and etoposide (60 mg/m^2) were given for 5 days every 4 weeks. After the induction chemotherapy, 24 Gy in 12 fractions in 3 weeks were given to the clinical target volume (CTV) as follows: for solitary germinomas, involved fields, or the initial gross tumor volume (GTV) with a two-dimensional (2D) margin of 2 cm; for multifocal germinoma, whole ventricles; and for disseminated germinoma, whole central nervous system (CNS). The CTV was not altered by the level of serum HCG-β. Within 2 weeks after the completion of the last course of chemotherapy, radiotherapy was started based on computed tomographic (CT) planning with slice-by-slice determination of the target volume. Magnetic resonance imaging (MRI) was used only as the reference, and no image fusion technique was used in the planning. No boost irradiation was used after the 24 Gy irradiation. First salvage treatment for the relapse was predetermined in the protocol as the same chemotherapy followed by whole brain or whole CNS irradiation of 24 Gy. Consequently, the maximum cumulative dose is then 48 Gy to the initial PTV and 24 Gy to the whole brain or whole CNS, respectively, if tumors relapse in patients who have already been treated with focal volume as the initial treatment. Six or 10 MV X-rays were used with multiple portals for the involved fields, parallel opposed fields for the whole ventricles and whole brain, and posterior tandem fields for the whole spinal irradiation, respectively.

Treatment planning was performed with Therac (NEC, Tokyo, Japan) from 1992–1995, and with Focus (CMS Japan, Tokyo, Japan) after 1995. Three-dimensional dose distribution was available for the transaxial, coronal, and sagittal views at the isocenter for patients who were treated with involved fields or whole ventricle fields. The concept of planning target volume (PTV) and CTV was not well understood at the start of this study, and CTV was covered by the isodose curve of 90% of the dose prescribed at the isocenter. In the present study, all CT and MRI slices before surgery/chemotherapy and those for radiotherapy planning were retrospectively reviewed for all the patients entered in the study. A radiation oncologist (H.A.) surveyed the 2D minimum distance between the tumor size before surgery/induction chemotherapy and the 90% isodose surface. The retrospective review was based on the careful visual correlation between planning-based CT and the diagnostic CT or MRI studies but not on image fusion techniques. The serum HCG-β was blinded to the investigator at the time of analysis. For the comparison between two categories, the chi-square test was used. Kaplan-Meier analysis and the log-rank test were used for the survival analysis.

Table 1. Information on the 6 patients who experienced tumor relapse

Serum HCG-β (mIU/mL)		TV	Site of failure relative to TV	Spinal relapse
Elevated				
1	101	Local	Outside	
2	233	Local	Margin	
3	0.7	Local	Outside	Yes
4	5.3	Local	Outside	
5	0.7	Local	In and outside	
Nonelevated				
6	<0.5	Local	Outside	Yes

Abbreviations: HCG = human chorionic gonadotropin; TV = treated volume.

RESULTS

Between February 1992 and November 1999, 27 patients were entered in the study, as reported in the previous article (7). Age was 15.7 years old at median, distributed from 8–28 years. Twenty patients were 18 years old or younger and 7 patients were more than 18 years old. Cytology of craniospinal fluid, enhanced cranial MRI, and enhanced spinal MRI were used in staging work-up in all patients. The follow-up period was 58 months at median, ranging from 18–102 months. All but 1 patient was followed more than 24 months. Sixteen patients showed a normal serum HCG-β level, which was < 0.5 mIU/mL in our institution, and 11 patients showed elevated HCG-β with the mean at 7.4 mIU/mL, and the range from 0.7–233 mIU/mL. Serum HCG-β was elevated in 8 of the 18 patients with solitary tumors, 2 of the 6 patients with multifocal tumors, and 1 of the 3 patients with disseminated tumors. These were all treated with 24 Gy in 12 fractions in 3 weeks for the involved fields, whole ventricle, and whole CNS irradiation, respectively.

The disease-specific survival at 5 years was 100%, and the overall survival was 95%. The relapse-free survival at 5 years, according to the serum HCG-β level, was 90% for patients with normal HCG-β and 44% for patients with elevated serum HCG-β ($p = 0.025$). When we allowed for the first salvage treatment administered when relapse occurred, the tumor control rate was 95% at 5 years.

Details on the patients who experienced treatment failure are shown in Table 1. Five of 6 relapses were observed in patients with elevated serum HCG-β. All patients were treated with involved fields. The site of failure relative to the treated volume (TV), covered by 90% of the prescribed dose, was outside the TV in 4 (2 had spinal lesions), the marginal site in 1, and outside and in the TV (2 relapses) in 1 patient. Therefore, the local failure rate was 3.7% for the

Table 2. Relationship between the serum HCG-β, treated volume, and disease control in 27 patients with intracranial germinoma

Clinical subtype	Treated volume			
	Local	WV	WCNS	Total
Total	12/18	6/6	3/3	21/27
Serum HCG-β <0.5 mIU/mL	9/10	4/4	2/2	15/16
Serum HCG-β elevated	3/8	2/2	1/1	6/11

Abbreviations: HCG = human chorionic gonadotropin; WV = whole ventricle; WCNS = whole central nervous system.

definite in-field relapse, and 7.4% for the marginal or in-field relapse.

Table 2 shows the relationship between the serum HCG-β, treated volume, and relapse ratio. There were no relapses in 9 patients who were treated for whole ventricle or whole CNS. A small treatment volume and elevated serum HCG-β were equally considered candidates for causing the poor local control.

Even though the 2D margin for the initial GTV was determined to be 2.0 cm or more in the protocol, 12 of 27 patients were treated with < 2.0 cm, and 10 with < 1.5 cm margin. Most tumors were very small or not visible in the planning CT and MRI at the time of radiotherapy, because of the efficacy of the induction chemotherapy. All 6 relapses were treated with a 2D margin <1.5 cm. There were no relapses in 4 patients who had elevated serum HCG-β and who were treated with whole ventricle or larger fields. The whole ventricle field included the fourth ventricle. There was a statistically significant difference in the relapse ratio between patients treated with a 2D margin < 1.5 cm (median, 1.0 cm; range, 0.5 1.2 cm), and those with a 2D margin > 1.5 cm (median, 2.4 cm; range, 1.5 2.8 cm; $p < 0.01$; Table 3).

The complications due to treatment were azoospermina in 1 of 4 patients examined. One patient experienced anterior pituitary hormonal replacement owing to relapse at the neurohypophyseal region. No new onset or deterioration in anterior pituitary function was noted. Three of 7 adult patients older than 18 years at the time of treatment married after treatment, and 1 fathered a child.

Table 3. Relationship between serum HCG-β, 2D margin, and relapse ratio in 27 patients with intracranial germinoma

Serum HCG-β	2D margin <1.5 cm	2D margin >1.5 cm
<0.5 mIU/mg	1/3	0/13
>0.5 mIU/mg	5/7	0/4

Abbreviations: HCG = human chorionic gonadotropin; 2D = two-dimensional.

DISCUSSION

It is well known that localized treated volume results in a high relapse rate in intracranial germinoma. In a multi-institutional retrospective survey, Aoyama *et al.* (9) showed that the 5-year relapse-free rate was significantly lower in patients treated with localized volume than whole ventricle or larger volume. Because a high incidence of radiation-related late complications have been noted after large volume irradiation for pediatric patients, induction chemotherapy has been expected to reduce the amount of radiation volume and dose. There are pros and cons to this opinion (3 5, 10 14). The possible incidence of relapses using lower doses and smaller volumes is the shortcoming of this approach to this highly curable disease. Pretreatment impairment in neurocognitive function due to the tumor or surgery is also suggested to be a possible bias in the opinion against radiotherapy (15, 16). The lack of well-controlled randomized trials and the small number of patients in each institution has forced us, at present, to conduct a careful analysis of the prospective Phase II studies to speculate on the best treatment method.

Elevated serum HCG-β was reported to be a poor prognostic factor for patients with intracranial germinoma treated with chemotherapy alone in a large multi-institutional study (11). We have analyzed our data to evaluate the prognostic importance of serum HCG-β based on the previous report, and found the possible importance of serum HCG-β in our series (7). A Japanese multi-institutional cooperative group began to treat intracranial germinoma with platinum-based induction chemotherapy followed by 24 Gy irradiation 6 years ago, and treated more than 100 patients. Preliminary reports of the large Phase II study suggested that HCG-β was not a prognostic factor, and that a smaller treatment volume was associated with a higher relapse rate (8).

The small number of patients in our study prevented us from determining whether elevated serum HCG-β or an inadequate CTV margin was the predominant prognostic factor. The patients with relapsed tumors were treated with a small margin, and also had a higher serum HCG-β. Notably, there were no relapses in patients who were treated with whole ventricle or a larger volume, despite the fact that these patients had a larger tumor burden than those who were treated with involved fields. The tumor mass before chemotherapy was often massive or infiltrative, but the tumor was very small or not visible at the time of treatment planning. These differences in size and the anatomic shift of the normal brain made it difficult to determine the appropriate CTV based on the initial GTV before surgery and chemotherapy. Image fusion between the initial MRI and treatment planning CT after chemotherapy would be difficult, because of the anatomic shift of the normal brain tissues. The high incidence of violation in using 2.0 cm margins for the initial GTV may be partly due to these limitations in modern diagnostic imaging techniques rather than inadequate skills on the part of the treating physicians.

Interobserver variation must be large, even when utilizing the advanced imaging technologies available at present. Therefore, it is still difficult to achieve good quality assurance and a good quality control program for using the involved field for intracranial germinoma in a multi-institutional study.

Considering the low relapse rate in the treated volume in this study, 3.7% 7.4%, induction chemotherapy may reduce the dose required for the eradication of gross tumors. We did not use any boost dose in this study or in the Japanese multi-institutional study. Recent studies in western countries show that physicians are still using a boost dose to the tumor bed, giving 40–50 Gy in total (10, 11). Our results suggest that a prospective multi-institutional study is needed to test whether a boost dose to the tumor bed is necessary. Elimination or reduction in the boost dose after 24 Gy has a high probability of reducing vascular complications and deterioration in the anterior pituitary function. It is necessary to carefully monitor the long-term adverse effects of chemotherapy. Reduction of the radiation dose without chemotherapy would also be an important subject for a multi-institutional study.

In conclusion, the relapse rate can be unacceptably high in patients who were treated with involved fields, partly because of the difficulty in accurately determining the initial GTV before surgery and chemotherapy. Although the total tumor control rate after initial salvage treatment was high, it is obvious that tumor relapse should be avoided. In this respect, whole ventricle or larger field is still the target volume, which should be regarded as the standard both for germinoma with normal HCG-β, and for germinoma with elevated HCG-β, both in chemoradiotherapy and in radiotherapy alone.

REFERENCES

1. Shirato H. Nishio M. Sawamura Y. *et al.* Analysis of long-term treatment of intracranial germinoma. *Int J Radiat Oncol Biol Phys* 1997;37:511–515.
2. Shibamoto Y. Abe M. Yamashita J. *et al.* Treatment results of intracranial germinoma as a function of the irradiated volume. *Int J Radiat Oncol Biol Phys* 1988;15:285–290.
3. Wolden SK. Wara WM. Larson DA. *et al.* Radiation therapy for primary intracranial germ-cell tumors. *Int J Radiat Oncol Biol Phys* 1995;32:943–949.
4. Merchant TE. Sherwood SH. Mulhern RK. *et al.* CNS germinoma: Disease control and long-term functional outcome for 12 children treated with craniospinal irradiation. *Int J Radiat Oncol Biol Phys* 2000;46:1171–1176.
5. Allen JC. DaRosso RC. Donahue B. Nirenberg A. A phase II trial of preirradiation carboplatin in newly diagnosed germinoma of the central nervous system. *Cancer* 1994;74:940–944.
6. Sawamura Y. Shirato H. Ikeda J. *et al.* Induction chemotherapy followed by reduced-volume radiation therapy for newly diagnosed central nervous system germinoma. *J Neurosurg* 1998;88:66–72.
7. Aoyama H. Shirato H. Ikeda J. *et al.* Induction chemotherapy followed by low-dose involved field radiotherapy for intracranial germ cell tumors. *J Clin Oncol* 2002;20:857–865.
8. Matsutani M. for the Japanese Pediatric Brain Tumor Study Group. Combined chemotherapy and radiation therapy for CNS germ cell tumors—the Japanese experience. *J Neurooncol* 2001;54:311–316.
9. Aoyama H. Shirato H. Kakuto Y. *et al.* Pathologically-proven intracranial germinoma treated by radiation therapy. Radiother Oncol 1998;47:201–205.
10. Bamberg M. Kortmann RD. Calaminus G. *et al.* Radiation therapy for intracranial germinoma: Results of the German cooperative prospective trial MAIKEI 83/86/89. *J Clin Oncol* 1999;17:2585–2592.
11. Balmaceda C. Heller G. Rosenblum M. *et al.* Chemotherapy without irradiation—a novel approach for newly diagnosed CNS germ cell tumors: Results of an international cooperative trial. *J Clin Oncol* 1996;14:2908–2915.
12. Merchant TE. Davis BJ. Sheldon JM. *et al.* Radiation therapy for relapsed CNS germinoma after primary chemotherapy. *J Clin Oncol* 1998;16:204–209.
13. Lindstadt D. Wara WM. Edwards MSB. *et al.* Radiotherapy of primary intracranial germinoma: The case against routine craniospinal irradiation. *Int J Radiat Oncol Biol Phys* 1998;15:291–297.
14. Buckner JC. Peethambaram PP. Smithson WA. *et al.* Phase II trial of primary chemotherapy followed by reduced-dose radiation for CNS germ cell tumor. *J Clin Oncol* 1999;17:933–940.
15. Kitamura K. Shirato H. Sawamura Y. *et al.* Preirradiation evaluation and technical assessment of involved field radiotherapy using computed tomographic (CT) simulation and neoadjuvant chemotherapy for intracranial germinoma. *Int J Radiat Oncol Biol Phys* 1999;43:783–788.
16. Sutton LN. Radcliffe J. Goldwein JW. *et al.* Quality of life of adult survivors of germinomas treated with craniospinal irradiation. *Neurosurgery* 1999;46:1292–1298.

Int. J. Radiation Oncology Biol. Phys., Vol. 60, No. 1, pp. 335–341, 2004

0360-3016/04/$–see front matter

ELSEVIER

doi:10.1016/j.ijrobp.2004.04.028

PHYSICS CONTRIBUTION

FEASIBILITY OF SYNCHRONIZATION OF REAL-TIME TUMOR-TRACKING RADIOTHERAPY AND INTENSITY-MODULATED RADIOTHERAPY FROM VIEWPOINT OF EXCESSIVE DOSE FROM FLUOROSCOPY

HIROKI SHIRATO, M.D., PH.D., MASATAKA OITA, R.T., KATSUHISA FUJITA, R.T., YOSHIHARU WATANABE, R.T., AND KAZUO MIYASAKA, M.D., PH.D.

Department of Radiology, Hokkaido University Hospital, Sapporo, Japan

Purpose: Synchronization of the techniques in real-time tumor-tracking radiotherapy (RTRT) and intensity-modulated RT (IMRT) is expected to be useful for the treatment of tumors in motion. Our goal was to estimate the feasibility of the synchronization from the viewpoint of excessive dose resulting from the use of fluoroscopy.
Methods and Materials: Using an ionization chamber for diagnostic X-rays, we measured the air kerma rate, surface dose with backscatter, and dose distribution in depth in a solid phantom from a fluoroscopic RTRT system. A nominal 50–120 kilovoltage peak (kVp) of X-ray energy and a nominal 1–4 ms of pulse width were used in the measurements.
Results: The mean ± SD air kerma rate from one fluoroscope was 238.8 ± 0.54 mGy/h for a nominal pulse width of 2.0 ms and nominal 100 kVp of X-ray energy at the isocenter of the linear accelerator. The air kerma rate increased steeply with the increase in the X-ray beam energy. The surface dose was 28–980 mGy/h. The absorbed dose at a 5.0-cm depth in the phantom was 37–58% of the peak dose. The estimated skin surface dose from one fluoroscope in RTRT was 29–1182 mGy/h and was strongly dependent on the kilovoltage peak and pulse width of the fluoroscope and slightly dependent on the distance between the skin and isocenter.
Conclusion: The skin surface dose and absorbed depth dose resulting from fluoroscopy during RTRT can be significant if RTRT is synchronized with IMRT using a multileaf collimator. Precise estimation of the absorbed dose from fluoroscopy during RT and approaches to reduce the amount of exposure are mandatory.

Real-time tumor-tracking radiotherapy, Fluoroscopy, Dosimetry.

INTRODUCTION

Fluoroscopic detection of internal fiducial markers for precise setup of patients has been shown to be useful for static radiotherapy (RT) (1–5) and real-time tracking and gated RT (6–10). Prototype real-time tumor-tracking RT (RTRT) uses two sets of fluoroscopy to detect the internal motion of a metallic fiducial marker in or near the target volume (1). Attention to four-dimensional accuracy in space and time is increasing for tumors in motion when the meticulous dose distribution used in particle therapy (11) and intensity-modulated RT (IMRT) (12–17). Synchronization of IMRT and RTRT is expected to increase the therapeutic ratio for tracking moving tumors.

In our previous studies of RTRT without IMRT, the dose rate in the phantom was measured with thermoluminescence and a surface dosimeter (12, 16). The dose rate at 120 kV with a pulse width of 4 ms was 10.8 mGy/min at the entrance. We concluded that the fluoroscopic dose is negligible for patients treated with 60 Gy to the isocenter. However, because the beam-on time will be longer when we combine RTRT with IMRT using a multileaf collimator, integration of IMRT and RTRT could result in an extremely long treatment time. IMRT using a multileaf collimator requires a radiation time four to five times longer than conventional RT. This may result in unacceptable exposure from the fluoroscopy.

Interventional neuroradiology requires fluoroscopic examination for >30 min, on average, and is known to result in a noticeably high skin dose (18). Gkanatsios *et al.* (19) have shown that the median surface dose during a neuroradiologic diagnostic imaging examination is 1.3 Gy, with a maximal surface dose as great as 5.1 Gy.

These results suggest the importance of precise dose measurement in RTRT when the treatment time needs to be longer than previously estimated. We measured the dose resulting from the use of fluoroscopy in the RTRT system.

Reprint requests to: Hiroki Shirato, M.D., Ph.D., Department of Radiology, Hokkaido University School of Medicine, North-15 West-7, Kita-ku, Sapporo 006-8638, Japan. Tel: (+81)11-706-5975; Fax (+81) 11-706-7876; E-mail: hshirato@radi.med.hokudai.ac.jp

Partly supported by a grant-in-aid from the Japanese Ministry of Education, Sports, Culture, and Science.

Received Oct 21, 2003, and in revised form Apr 2, 2004. Accepted for publication Apr 5, 2004.

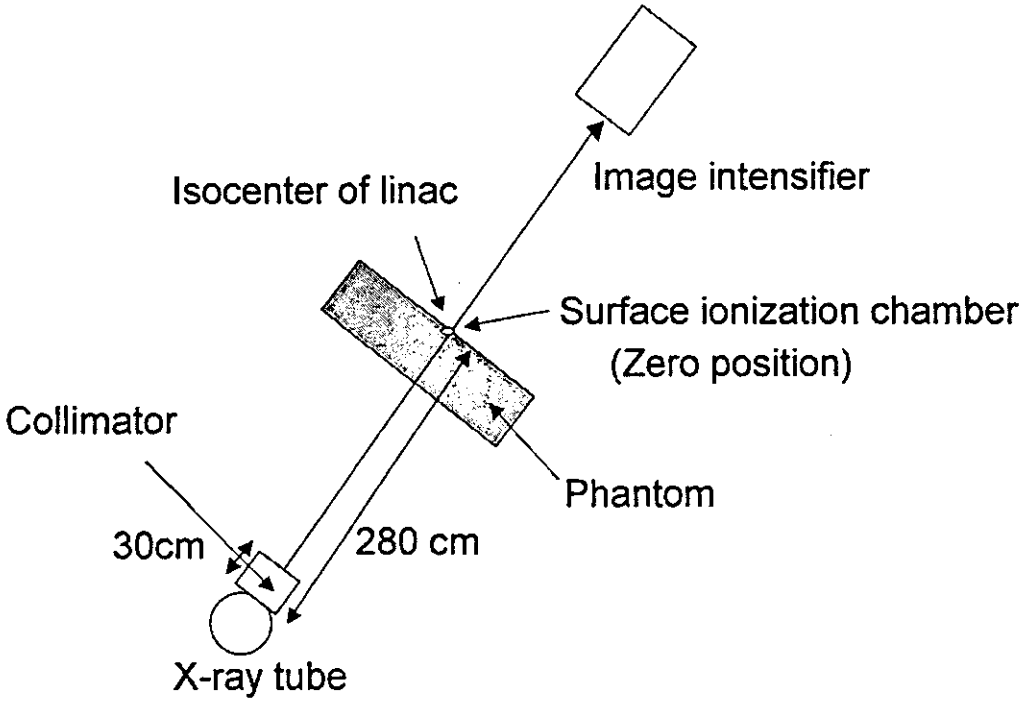

Fig. 1. Geometry of experiments used in this study. Linac = linear accelerator.

METHODS AND MATERIALS

Fluoroscopy

The fluoroscope was a rotating anode X-ray tube assembly (G-1582 BI, Shimadzu, Kyoto, Japan) powered by a three-phase generator. Photons were produced by a 0.6 × 0.6 mm^2 nominal size electron beam incident on a rotating target. We used a pulsed cathode of 80 mA, because it is commonly used clinically. For peak tube potentials of 50–120 kilovoltage peak (kVp), the pulse rate used was a nominal 30 s, with pulse duration of 1.2, 1.6, 2.0, 2.5, and 3.2 ms. The power of the X-ray tube was 1500 kJ for a 0.6-mm focus and 1060 kJ for a 1.0-mm focus. The inherent X-ray filtration was 1.5 mm aluminum equivalent.

The geometries of the fluoroscopy and measurement are shown in Fig. 1. The X-ray beam was collimated to visualize the image of the fiducial markers, which should be placed close to the isocenter. The distance from the X-ray tube to the image detector was 460 cm to avoid collision between the image detectors and the gantry of the linear accelerator. The distance from the X-ray tube (target) to the isocenter of the linear accelerator was 280 cm. The fluoroscopic beam was collimated to 1.6 × 1.9 cm at a 30-cm distance from the tube. The beam size enlarged to 14.5 × 18.5 cm^2 at the isocenter of the linear accelerator where the measurement was performed.

Measurement

The fluoroscopy irradiated field was measured in air using film at the plane including the isocenter perpendicular to the beam axis of the diagnostic X-ray.

The air kerma was measured with a cylindrical chamber with a collecting volume of 3 cm^3, using a Scanditronix WELLHOFER DC300 TNC/160 and a RAMTEC 1500B (Toyo Medic, Tokyo, Japan) designed for diagnostic radiography and mammography. The nominal X-ray energy available for measurement was quoted as 20–150 kV. The wall of the chamber was made of Shonka C552 (1.7 g/cm^3) with the thickness at 0.3 mm. The chamber has an outer length of 41.5 mm and an outer diameter of 10.6 mm. The nominal calibration factor was 9.3 mGy/nC.

The half value layer was measured using varying thicknesses (0.25, 1.05, and 2.05 mm) of a 20.0 × 30.0-cm aluminum (Al) sheet (99.999% Al). The half value layer was measured using a source-to-aluminum filtration distance of 25 cm and a source-to-detector distance of 280 cm.

The dose in air at the isocenter was measured to estimate the air kerma, which does not take into account any backscatter. The distance from the X-ray source to the central axis of the chamber was 280 cm, and the field size was 10 × 14 cm^2. The chamber was positioned on the central axis of the beam, with its long axes parallel to the cathode–anode direction of the X-ray tube.

The percent depth dose (PDD) was measured with a smaller chamber, a farmer-type chamber No. 2591 with a collecting volume of 0.6 cm^3 without a build-up cap in the Solid Water phantom. The ionization chamber was placed on the surface of the phantom, which consisted of 30 × 30-cm^2 slabs of Solid Water, with a total thickness of 10 cm (Fig. 1). The source-to-surface distance was set at 280 cm from the tube. The dose rate at 0.0, 1.0, 2.0, 3.0, 4.0, 5.0, 6.0, 8.0, 10, 12, 15, and 20 cm was measured by changing the depth of the chamber perpendicular to the beam axis for

Table 1. Measured air kerma rate from one fluoroscope at isocenter of linear accelerator according to nominal kVp

	Nominal kVp			
Air kerma rate	50	70	100	120
Mean (mGy/h)	33.50	90.25	238.80	366.18
SD (mGy/h)	0.30	0.15	0.54	0.86
%SD	0.9	0.2	0.2	0.2

Abbreviation: kVp = kilovoltage peak.

a nominal 50-, 70-, 100-, and 120-kVp X-ray beam, respectively. The depth of the camber was adjusted by adding the corresponding 30 × 30-cm^2 slabs of Solid Water, with a total thickness of 1.0–20 cm on the surface of the phantom. The position of the chamber was adjusted to be on the central X-ray beam axis and parallel to the cathode–anode direction of the X-ray tube by visualizing the chamber under fluoroscopy. Correction was made for recombination, polarity, or energy dependence effects. The "surface" measurement at depth 0 was acquired with the center of the cylindrical chamber put at the same plane as the surface of the Solid Water phantom by cutting the surface of the phantom to fit it in. The PDD was normalized at the depth of the maximal dose for each X-ray beam.

The mean ± standard deviation were calculated for each data item on the basis of 10 measurements for each data point.

RESULTS

The half-value layer for each nominal kilovoltage peak of the X-ray tube was estimated to be 2.73, 3.71, 5.02, and 6.72 mm Al for a nominal 50, 70, 100, and 120-kVp X-ray beam, respectively.

The air kerma rate from one fluoroscope was 20.3 ± 0.2, 26.3 ± 0.4, 33.5 ± 0.3, 47.9 ± 0.2, and 68.2 ± 0.3 mGy/h at a nominal pulse width of 1.2, 1.6, 2.0, 2.8, and 4.0 ms, respectively, with a nominal 50-kVp X-ray beam. The air kerma rate from simultaneous exposure of two fluoroscopes with a nominal 50-kVp X-ray beam for 1.6 and 2.0 ms was 58.7 ± 0.5 and 72.7 ± 0.3 Gy/h respectively, which was roughly twice (2.2 times the rate with one fluoroscope) the corresponding dose rate of one fluoroscope.

The air kerma rate measured for one X-ray tube at the isocenter of the linear accelerator is shown in Table 1 for each nominal kilovoltage peak of the X-ray tube using 2.0 ms as the pulse width. The air kerma rate from one fluoroscope was 238.8 ± 0.54 mGy/h for a nominal pulse width of 2.0 ms with a nominal 100-kVp X-ray beam. The relationship between the nominal kilovoltage peak and the air kerma rate is shown in Fig. 2. The air kerma rate increased steeply with the increase in the X-ray beam energy.

The relationship between the pulse width and the surface dose rate, including backscatter, is shown in Fig. 3 according to the nominal kilovoltage peak. The surface dose was 28–980 mGy/h (Table 2). The surface dose was strongly dependent on the kilovoltage peak and linearly increased with the pulse width of the fluoroscope.

The PDD curves for each nominal kilovoltage peak of the X-ray beam are shown in Fig. 4. The dose at 5.0 cm was 37–58% for 50–120 kVp, respectively.

When we put a patient on the treatment couch, the patient's skin surface will receive a greater dose than the dose estimated at the isocenter because of the shorter distance from the X-ray source to the skin surface. Assuming that the distance between the skin entrance and the isocenter, r, is

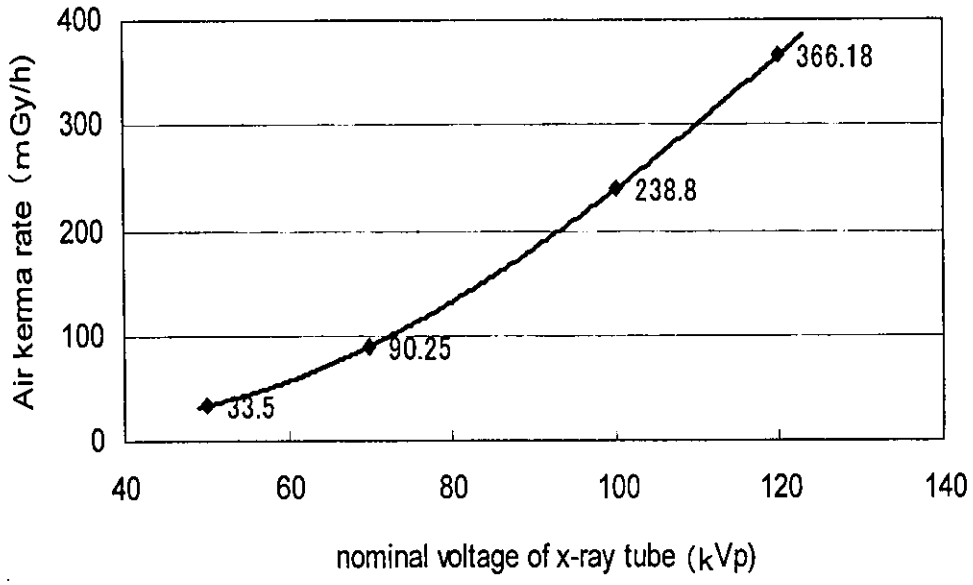

Fig. 2. Relationship between nominal kilovoltage peak of fluoroscopic X-ray and air kerma rate from one fluoroscope.

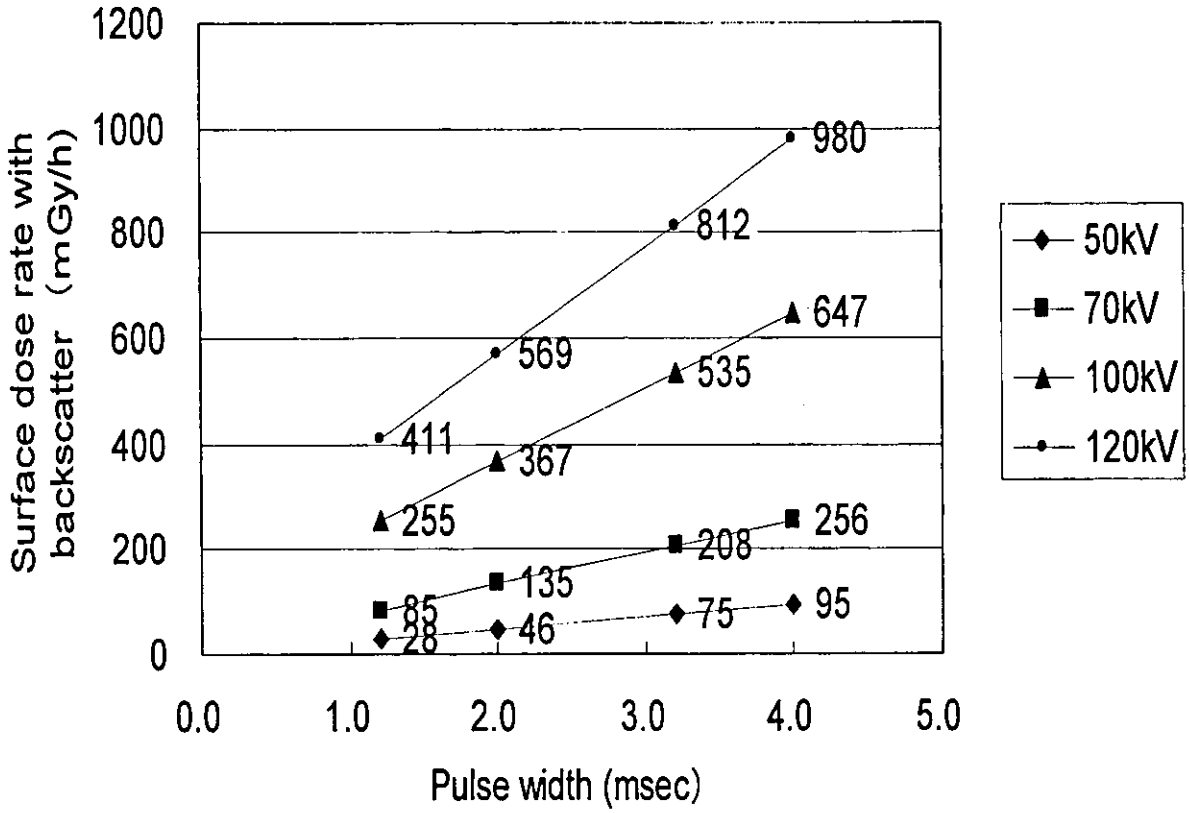

Fig. 3. Relationship between pulse width and surface dose rate from one fluoroscope according to kilovoltage peak. Diamonds, 50 kV; squares; 70 kV, triangles; 100 kV; circles, 120 kV.

5–25 cm, the estimated dose at the skin surface with backscatter (Fig. 5) will be from $r = 5$ cm to $r = 25$ cm. The dose was calculated simply using the formula $R^2/(Rr)^2$, where R is the distance from the X-ray source to the isocenter (280 cm in the RTRT system). The estimated skin surface dose from one fluoroscope in RTRT was 29–1182 mGy/h. The estimated skin surface dose was strongly dependent on the kilovoltage peak and the pulse width of the fluoroscope and slightly dependent on the distance between the skin and isocenter.

DISCUSSION

The Joint Working Party of the British Institute of Radiology and the Hospital Physicists' Association published PDD curves of similar beams measured for use in RT (20). Jennings and Harrison (21) and Harrison (22) have also published the depth dose of diagnostic radiography. Fetterly *et al.* (23) published the X-ray dose distribution of fluoroscopy beams in 2001. These data were based on the measurements using source-to-surface distances of 30–50 cm, far shorter than the source-to-surface distance of 280 cm used in the RTRT system. The greater percentage of dose at each depth in our study compared with those in previous reports for kilovoltage of X-rays may be a result of the longer source-to-surface distance in the RTRT system. We were not able to measure the "surface dose" by parallel chamber with sufficient sensitivity and used a 0.6-cm^3 cylindrical chamber, which could also have been a source of bias in our study. More work is required for precise measurement.

Table 2. Estimated dose rate at skin surface for different pulse widths and kVp values

Pulse width (ms)	Estimated dose rate (mGy/h)			
	50 kVp	70 kVp	100 kVp	120 kVp
1.2	28.4	483.2	255.2	411
2.0	45.9	762.2	366.8	568.5
3.2	75.4	1174.4	535	811.7
4.0	94.7	1448.7	647.4	980.1

Abbreviation: kVp = kilovoltage peak.

The real-time tumor-tracking system has been used with precise setup and gated RT in >200 patients with various tumors, including head-and-neck tumors and tumors of the lung, esophagus, liver, pancreas, prostate, and uterus (1). In this study, we investigated the parameters used in actual RTRT for various tumors. A nominal X-ray strength of 80 kVp and pulse width of 2–4 ms are frequently used for the head-and-neck region, and a strength of 100–120 kVp and duration of 2 ms are used for lung and liver treatment in clinical practice. If the patient's body is large or thick, the system requires 4 ms for visualization of the internal marker.